

	<h1 style="margin: 0;">SPIRE Test Report</h1>	<b>Ref: SPIRE-RAL-REP-002083</b> <b>Issue: DRAFT</b> <b>Date: 14 July 2004</b> <b>Page: 1 of 6</b>
CQM Cold Test 1 Performance Test Report Editor: Bruce Swinyard		

### Change notice

Issue	Date	Comment
Draft	14 July 2004	Draft issue for information for CDR – to be reviewed

## 0 Scope

This report covers the performance tests carried out on the CQM model of the SPIRE instrument during the first cooldown which took place at the RAL test facility from 2/2/04 until 13/2/04. The log of tests carried out can be found at [http://scott1.bnsc.rl.ac.uk:8080/hcss/test\\_area/Test\\_Log.htm](http://scott1.bnsc.rl.ac.uk:8080/hcss/test_area/Test_Log.htm) and the specification for the tests is given in SPIRE-RAL-NOT-001850.

### Reference Documents

RD1 CQM Performance Test Details – SPIRE-RAL-NOT-001850 v0.2

RD2 CQM Build Standard Spread Sheet – *to be numbered*

RD3 PLW CQM EIDP – SPIRE-JPL-DOC-002038

RD4 A Fourier Transform Spectrometer for Ground Testing of the Herschel SPIRE Instrument – Spencer *et al* SPIE paper

RD5 Analysis of Phase Shifted Loadcurves SPIRE-RAL-NOT-002094

## 1 Introduction

The CQM instrument consisted of the long wavelength photometer channel (PLW) with no operating mechanisms (see RD2). All photometer optics and optical filtering was flight representative as was the cooler and the photometer calibrator. There were no operating sub-systems in the spectrometer except for the calibrator. The PLW BDA was read out by a 48 channel JFET unit, all other JFET units were STMs with resistor networks representing the impedance of the detectors and JFET amplifiers.

The CQM PLW array was not of flight quality and testing at JPL (RD3) showed that there were six non-operable pixels and one non-operable thermistor on the array. Figure 1.1 shows the positions of the non-operable pixels and the numbering of the pixels used throughout this report.

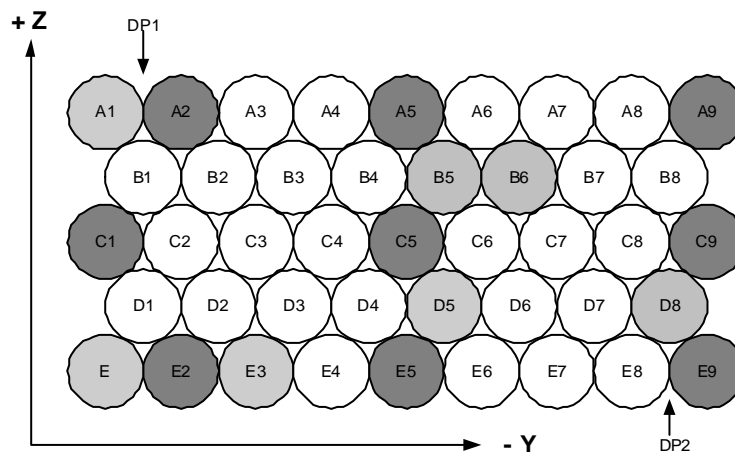


Figure 1.1: The CQM array, light shading indicates bad pixels and dark shading indicates those pixels used for optical testing.



## 2 Detector Tests

### 2.1 Noise Tests

The system noise was measured in several different ways to verify as many components of the system as possible.

**Shorted noise tests:** The first test carried out was using the operational JFET module with the detectors at 1.7 K thus effectively shorting the JFET inputs. This tests whether the warm electronics and/or the cryoharness are injecting excess noise into the system. It also allows the JFET noise as a function of applied bias to be tested.

**Biased Detector Tests:** Once the detectors reached operating temperature it was possible to test the noise as a function of applied bias under low background conditions. This is the ultimate test of the system performance. Under these circumstances it is also possible to look for 1/f type system noise to see whether there are any excess noise sources of a systematic rather than random nature.

**STM JFET Tests:** The resistor networks inside the STM JFET units allow us to test the noise as a function of applied detector bias but without the effect of the heating of the detector. This is a purer test of the electronic noise in the system. Again we can test both for the global noise level and for any 1/f type noise.

#### 2.1.1 Photometer JFET shorted input tests

The outline test configuration/procedure was as follows:

SPIRE CQM instrument in cryostat at nominal operating temperature

CQM P/LW JFET unit connected to QM1 DRCU via prime side test harness – the grounding links were left out for this test (see RD1 for comparison of in and out).

BDA at L0 interface temperature

$V_{dd}$  output 2.5V – actual 2.3 V as measured down redundant side of harness

$V_{ss}$  set to a variety of values between 0.5 and 3.9 V as measured at the DCU – there will be a ~200 mV drop down the harness

Signal collected for about 7 minutes

The analysis was done by dividing the time sequence data by  $V_{ss}$  setting and finding the standard deviation of the data in the time domain – this is divided by the square root of the band width (here 5 Hz) to give the noise in  $nV Hz^{1/2}$ . The results for each JFET membrane in the module (BD002 and BD 003 in module SN002) are shown in figure 2.1. There are clearly some channels with excess noise at some or all  $V_{ss}$  settings – there is no clear explanation for these. The time series and noise amplitude spectrum for the noisiest  $V_{ss}$  setting (1.9 V) for each of the good channels are shown side by side in figures 2.2a and 2.2b – we can see that there are periods of excess noise here. None of the consistently noisy channels shows excess noise when the detectors are at operating temperature see below so the most likely explanation is that these channels are picking up EMI due to the grounding links being left out for this test. We will confirm this during the next cooldown.



We can also see that where the channels are noisy that the noise originates before the low pass filter in the LIAs and is, therefore, associated with some external source. The fact that only some channels see it means that it is most likely pick up somewhere in the system.

Excluding the 3 consistently noisy channels on BD003, these data show that the shorted noise measured at instrument level is the same as measured at CEA. Those channels showing excess noise in this test do not show excess noise when the detectors were at operating temperature and functioning normally (RD1). I conclude that the excess noise is due to system level pick up from an unidentified external source and that the electronics are working essentially the same as tested by CEA.

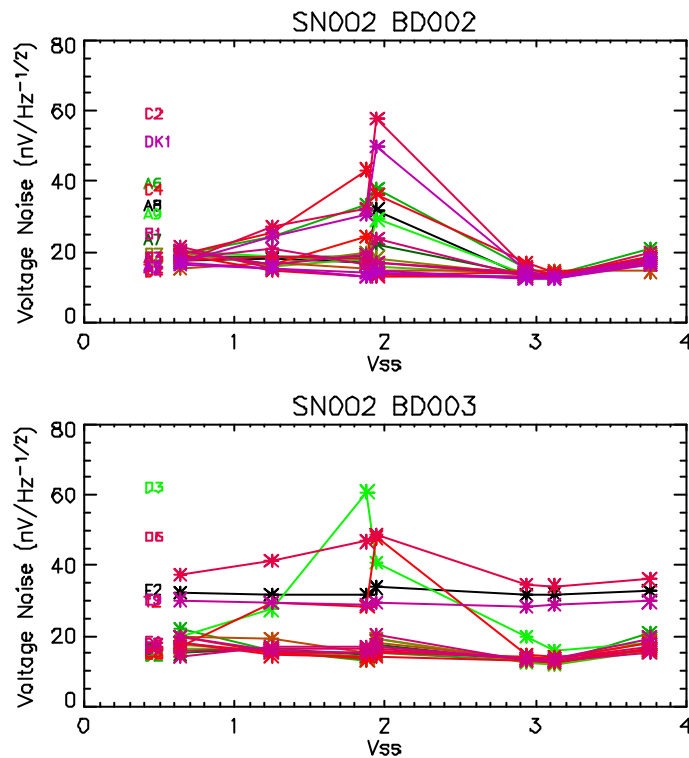


**Figure 2.1:** Time domain noise as a function of  $V_{ss}$  for each membrane. The “open” and “Bodac noisy” channels have been excluded from these data

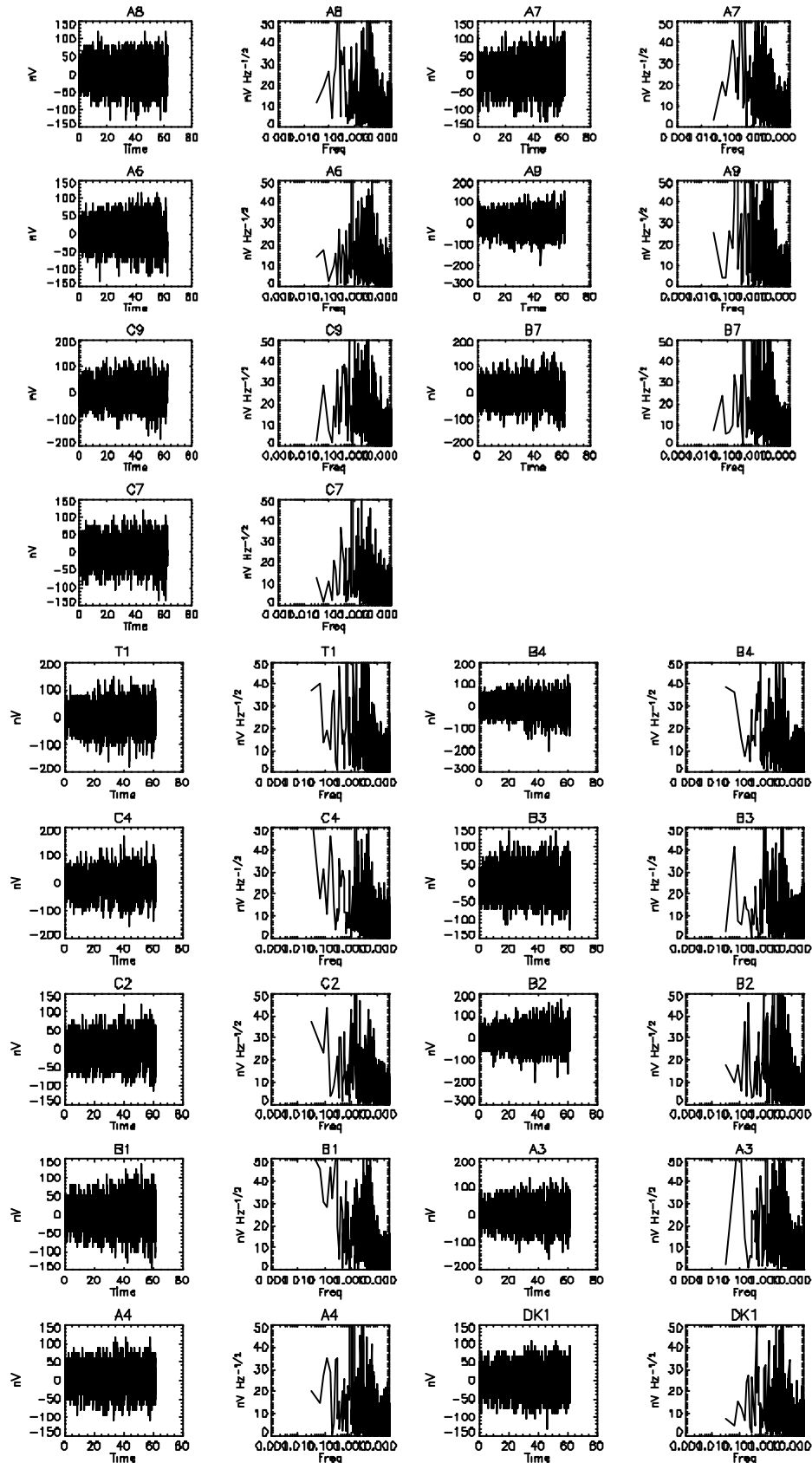


Figure 2.2a: Example of time domain and frequency domain noise spectra for BD002 – “Bodac noisy” channels excluded. This is for  $V_{ss} = 1.9$  V

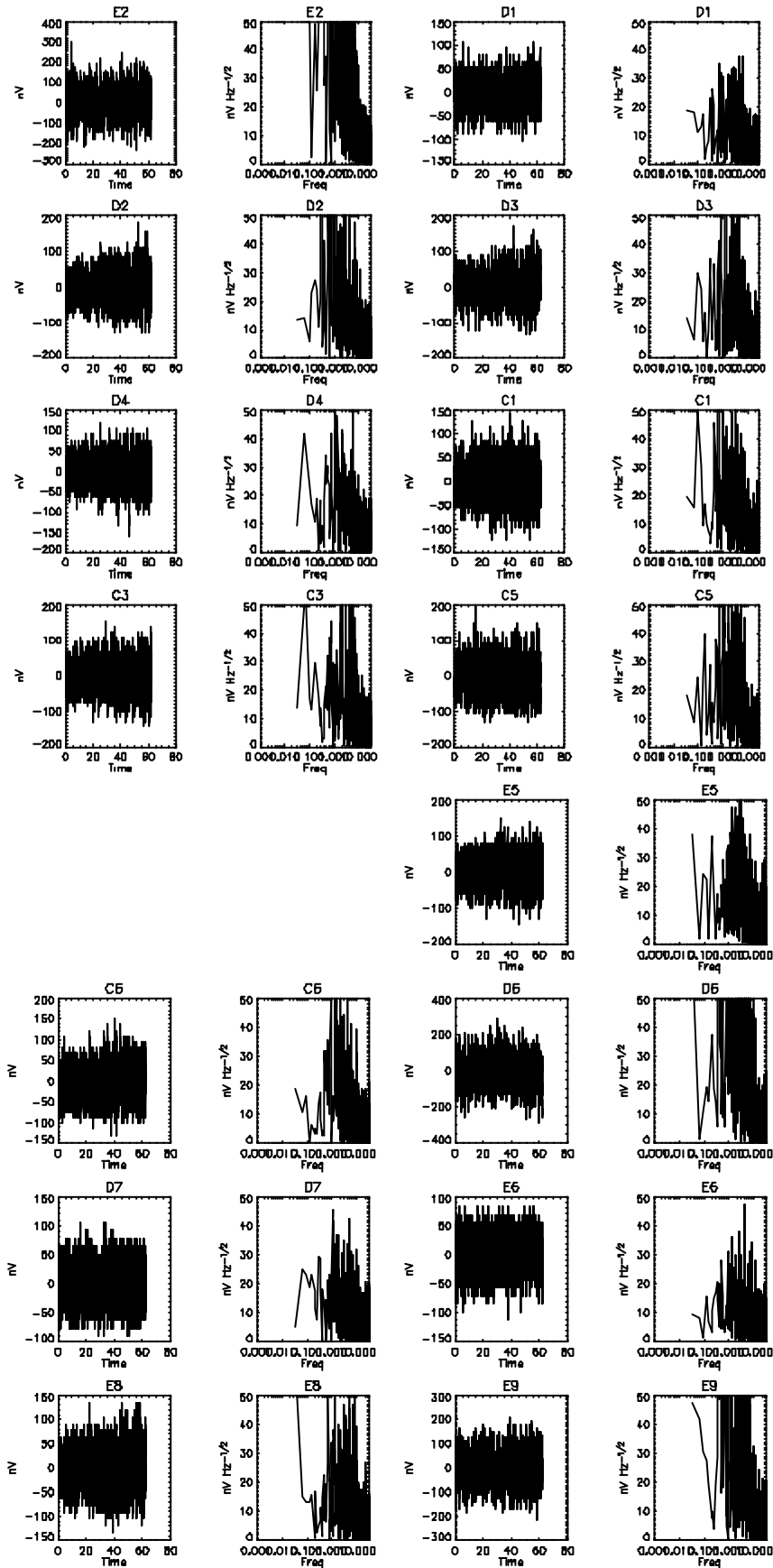


Figure 2.2b: Example of time domain and frequency domain noise spectra for BD003 – noisy channels excluded. This is for  $V_{SS} = 1.9$  V



### 2.1.2 Biased Detector Noise

The noise as a function of detector bias was tested with the CBB at its minimum temperature (~6.5 K) and therefore minimal loading on the detectors. The tests were performed at the bias frequencies, 70, 130 and 190 Hz. For each bias frequency 5 bias amplitudes were tested, 0, 4.94, 9.88, 15.10, and 29.92 Vrms and data were obtained for time periods of ten minutes per bias amplitude at 70 and 190 Hz and for five minutes per bias amplitude at 130 Hz. These tests were done prior to the change in the grounding scheme, which took place on 12/02/2004. Following the grounding change, the nominal bias frequency case was repeated for comparison and ten minutes of data per bias amplitude was taken.

We report here on the analysis of the 130 Hz data, there is no indication that there is any difference in the noise at different bias frequencies. The noise value was calculated from the average of the power spectrum over a 0.5 to 2.5 Hz range to avoid thermal drift and the cut on of the electrical filtering. This method was compared to calculating the RMS directly from the time line data for a single bias setting. The time domain calculated noise is on average a factor of 1.13 higher than the power spectrum calculation. Inspection of the power spectra showed no 1/f component due to electronic noise down to at least 0.03 Hz. There was evidence low frequency of thermal drifts in almost all noise data.

The results are depicted in Figures 2.3 and 2.4. The data from the noise tests at different bias amplitudes are shown as bar-diagrams. For each detector the left-most bar corresponds to 0 mV bias. There are 5 bars per detector with the bias increasing towards the right. The noise increases strongly for the first 3 bias levels and stays at the same level for the last two. Median noise levels over all pixels are given in Table T.

The noise determination in the time domain using the standard deviation and division by the square root of the upper band pass frequency is shown as pink symbols, appearing slightly above the corresponding 3<sup>rd</sup> bar. The green and blue triangles and circles respectively show the noise determined from the tests at assembly level. The median noise at the first instrument level tests is found to be 50% more than at assembly level tests, when comparing measurements at similar bias levels, i.e. 15.1 mV and 16 mV. However the noise determined from data taken after the grounding scheme of the test setup was changed to link the cryoharness shields in the flight configuration ("new gnd"), shown by black diamonds in the plot, indicates values very close to the ones measured at JPL.

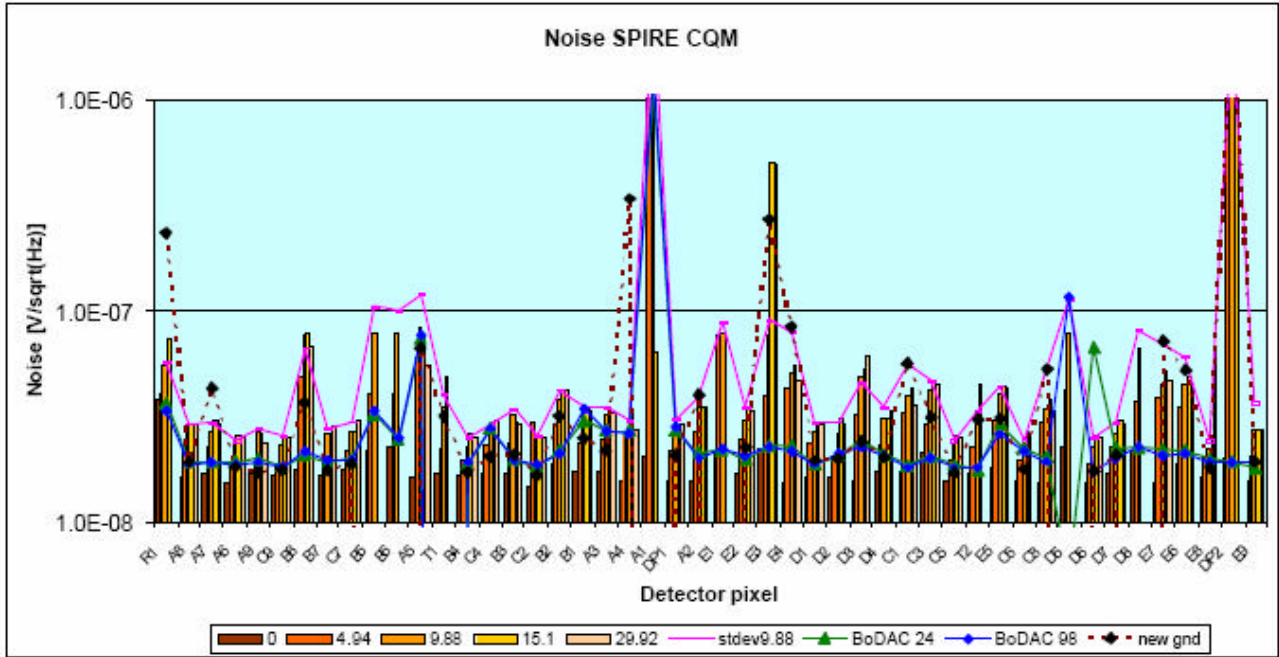


**Figure 2.4:** Measured noise in each detector channel as a function of applied bias for both the instrument level tests and unit level tests (labelled “BoDAC #”). The difference in the noise when the correct grounding configuration was implemented on the cryoharness is seen by the generally lower noise level on the points labelled “new gnd”.

Test Condition	Median Noise (nV Hz <sup>-1/2</sup> )
bias 0	16.9
bias 4.94 mV	24.2
bias 9.88 mV	31.7 (SD 34.9)
bias 15.1 mV	30.9
bias 29.92 mV	28.9
new gnd	20.7
BoDAC 24	20.9
BoDAC 98	20.5

**Table 2.1:** Median noise levels over all pixels in [nV Hz<sup>-1/2</sup>] for low background detector noise measurements at bias frequency of 130 Hz. See text for details.

### 2.1.3 Shorted Noise Tests on Spectrometer STM-JFETs

The outline test configuration/procedure was as follows:

STM spectrometer JFET units connected to QM1 DRCU via prime side test harness – the grounding links were left out for this test.

STM JFETs at 12 K

Bias applied 17, 35 and 70 mV rms

Offsets reset for each bias setting

Signal collected for about 13 minutes

The analysis was done by dividing the time sequence data by bias setting and finding the standard deviation of the data in the time domain – this is divided by the square root of the band width (here





25 Hz) to give the noise in  $\text{nV Hz}^{1/2}$ . In each STM JFET unit half the channels have the positive and negative terminals reversed meaning the signal becomes negative. Also one of the spectrometer LIA cards was disconnected owing to a fault in the harness. Therefore the noise was only analysed for 28 of the 72 LIA channels available.

The offset noise given by CEA for the photometer channels is  $132 \text{ nV}/\text{rt}(\text{Hz})$  at maximum offset setting (15) in a 5 Hz bandwidth. If we assume it is the same for the spectrometer side but with a 25 Hz bandwidth – scaling this gives  $59 \text{ nV}/\text{rt}(\text{Hz})$  at maximum offset setting. The offset noise is linearly proportional to offset setting – therefore we should get an additional  $3.9 \text{ nV}/\text{rt}(\text{Hz})$  per offset setting. Figure 2.5 shows a plot of the noise versus bias we would predict from the shorted channel (channel 0) if we add the noise in quadrature for the known offsets for the three bias settings (1,2 and 5) for the working channels. We can see that generally the increase in noise is as predicted for the offset circuit noise and there is no detectable excess noise due to the bias circuit.

The spectrometer LIAs have the same noise figure as tested by CEA (as shown by the shorted input). The increase in noise with increasing bias is essentially completely explained by the known fault of excess noise in the offset compensation circuit. Any noise due to the bias circuit itself must contribute less than  $1 \text{ nV}/\text{rt}(\text{Hz})$  maximum to the total noise figure. Some channels in this test set up show excess noise – the reason for this is not clear.

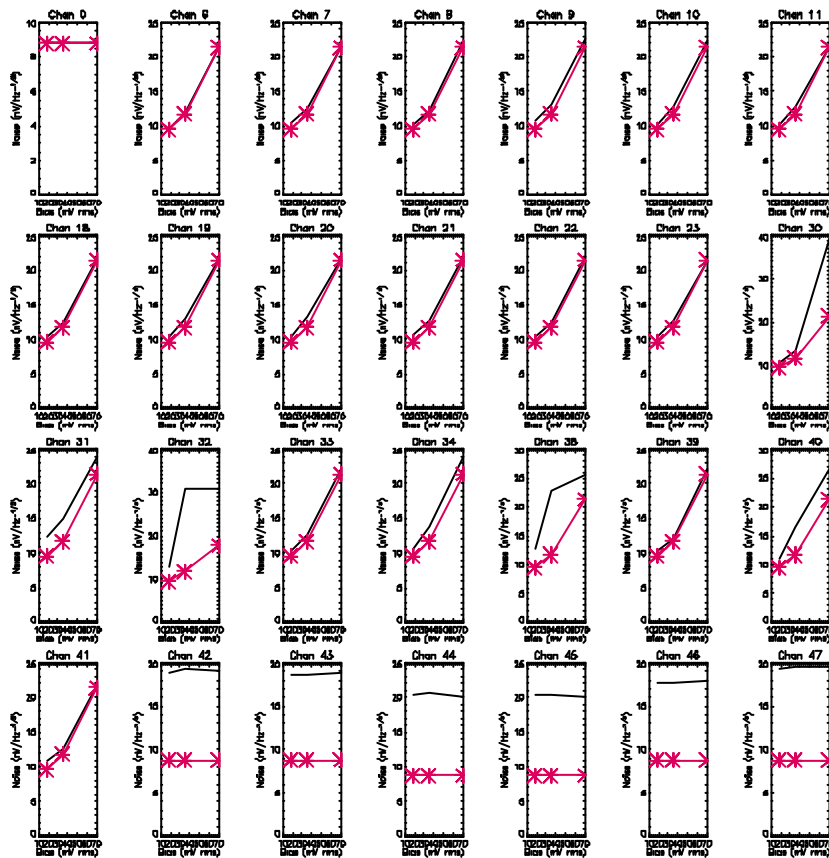


**Figure 2.5:** Noise taken in the time domain as a function of bias setting for the connected spectrometer JFET-STM channels (black line). Note channel 0 has a shorted input. The red line with stars shows the predicted noise taking the proportional noise from the offset circuit and adding in quadrature to the shorted input noise figure at each bias setting. Channels 42 to 47 show anomalous behaviour that has yet to be explained.





## 2.2 Loadcurve

Load curves (measurements of the bolometer voltage as a function of current) enable parameters describing the electrical and thermal properties of a bolometer to be determined. The performance of the bolometer can then be predicted for different operating conditions. Load curves can also be used to calculate the optical power absorbed by a bolometer.

Load curves are conventionally measured using a DC bias. However, for these tests the flight electronics were used; for performance reasons these use an AC bias. In order to determine that we were correctly compensating for frequency dependent effects, load curves were measured using several bias frequencies, and the in and out of phase detector voltage was measured (see RD5). The load curves measured at different frequencies were in good agreement once they had been corrected for frequency dependent effects. Load curves have previously been measured using a DC bias on this array at JPL before it was shipped for integration with the instrument.

Loadcurves were taken under a number of operating conditions during instrument level testing, these are summarised here:

### Load conditions

Minimum background (CBB ~6.5 K)

CBB at 8.5 K

CBB at 11.3 K

Viewing ambient background in room

### Bias Conditions

70 Hz in and out of phase

130 Hz in and out of phase

190 Hz in and out of phase

130 Hz in phase

130 Hz in phase

130 Hz in phase

Figure 2.6 shows load curves measured on one bolometer from the array, at different black body temperatures. The effect of loading from the black body can clearly be seen as a depression of the measured voltage. Results from the other bolometers were similar. The lines show the results of fitting the ideal bolometer model to the measured data the model produced good fits to all operating bolometers in the array, demonstrating that all the bolometers are well behaved. The model requires the bolometer resistance to be known as a function of temperature; the range of temperatures available in these tests did not permit this to be determined, and values measured on the array at JPL were therefore used. The model gives values of parameters describing the thermal conductance between the bolometer absorber and heat sink; these were in good agreement with the values measured at JPL.

The loadcurve data are still being analysed in order to understand the differences between the AC and DC cases. We can make some preliminary conclusions:

- The bolometers work the same way in the instrument as during unit level tests
- There is no excess background in the cryostat when the flip mirror is viewing the CBB
- The background from the ambient room is gives the same power onto the detectors as the CBB at 8.5 K. This is as expected from the the calculation using the measured filter profiles.
- There is a difference in the derived detector parameters from the unit level tests and the instrument level tests. This is either associated with poor knowledge of the absolute temperatures in the two situations or with the correction between AC and DC bias conditions.

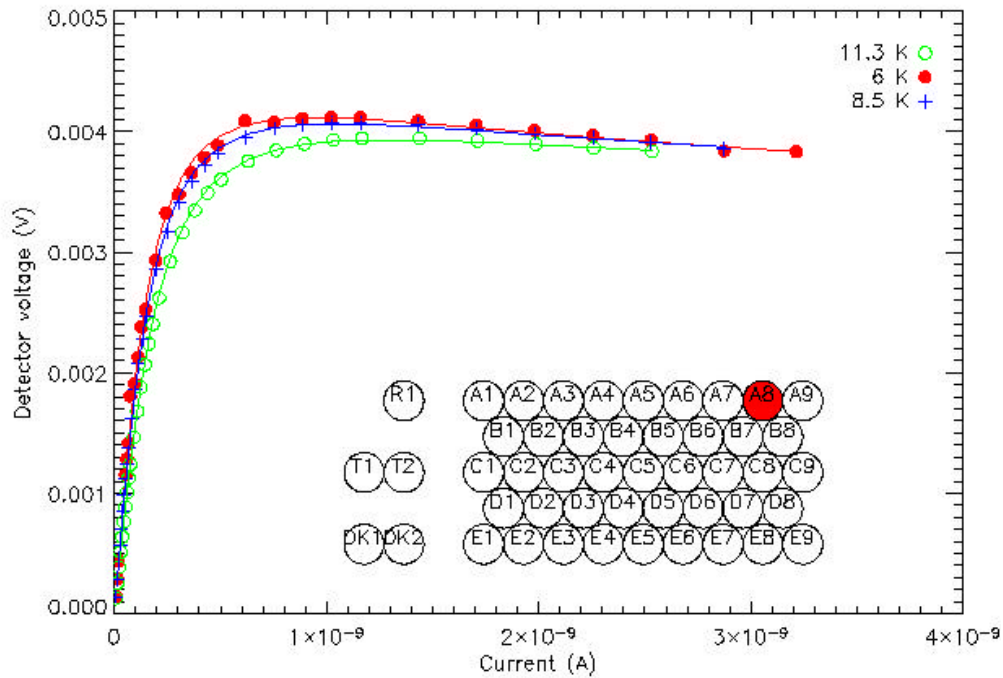
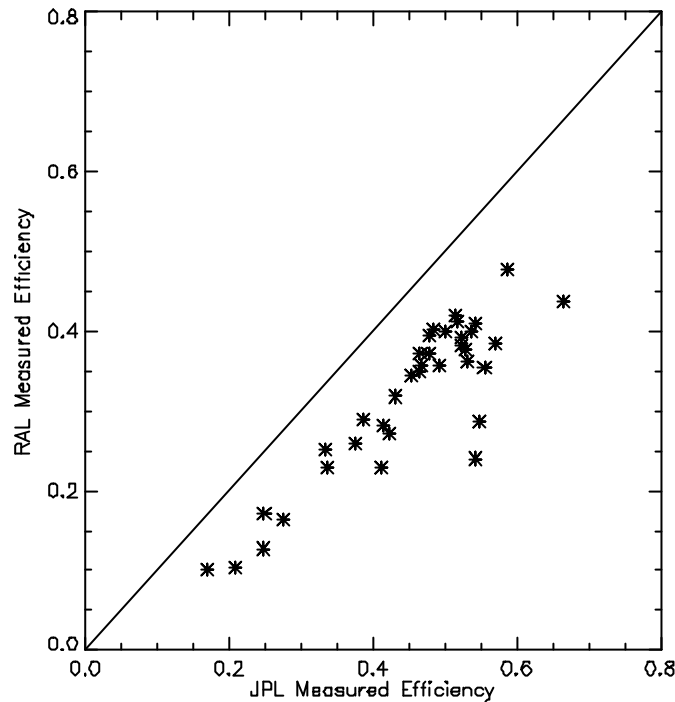


Figure 2.6. Load curves for detector A8 viewing the black body at different temperatures.

### 2.3 Optical Efficiency

The overall optical efficiency of the instrument can be measured by comparing the temperature rise seen with the CBB at two different temperatures and calculating the absorbed power using the detector thermal conductivity ( $G_0$ ) measured on the array at unit level. Data were obtained with the CBB at 8.5 K and 11 K. By subtracting the 8.5-K measured power from the 11-K measured power and dividing by the expected power using knowledge of the instrument passband from the measurement of the individual filters and making some assumptions about the instrument throughput and black body emissivity, we can calculate the optical efficiency of the detectors and compare it to that measured during array testing at JPL. Figure 6 shows the comparison between the RAL and the JPL measurements. The general trend is reproduced between the two measurements to within 20% (the RAL figures being systematically lower than the JPL figures). This difference could be due to a number of factors in the calculations from the data from either measurement. There is clearly more work to be done to understand the difference, but the results have demonstrated that the overall efficiency of the optics and filters is within specification.



**Figure 2.7:** Comparison of JPL quoted optical efficiency from unit level tests and that calculated using power difference between 8.5 and 11 K black body and predicted power assuming  $\tau = 0.2$  throughput with 0.5 transmission efficiency for filters; 0.9 emissivity for blackbody and 0.86 for truncation at cold stop. We assume the spectral response from the filter profiles and a sharp waveguide cut at 16.7 cm<sup>-1</sup>.

## 2.4 Frequency Response Test

On xxx the detector response to different chop frequencies was characterised. This was done by illuminating pixel C5 with the hot blackbody and then setting the chopper to 2,6,4,10,5,2,4,8,16,32,12, and 1 Hz in turn. A few minutes of chopped data was taken at each chop frequency.

The data were demodulated by multiplying by a sine and cosine of the same frequency. The signal vs frequency plot is shown in figure 2.8. Two of the frequencies (5Hz and 12Hz) yielded bad data and the cause of this is under investigation. For this detector, the  $f_{3db}$  point is at about 5 Hz.

The results from this test show that it is an adequate test to determine the detector time constant and further analysis on all detectors will be done to correlate the results with the expected response. This test was also done using the laser as a source and these data have not yet been analysed. During the next round of testing this test will be repeated with more pixels tested.

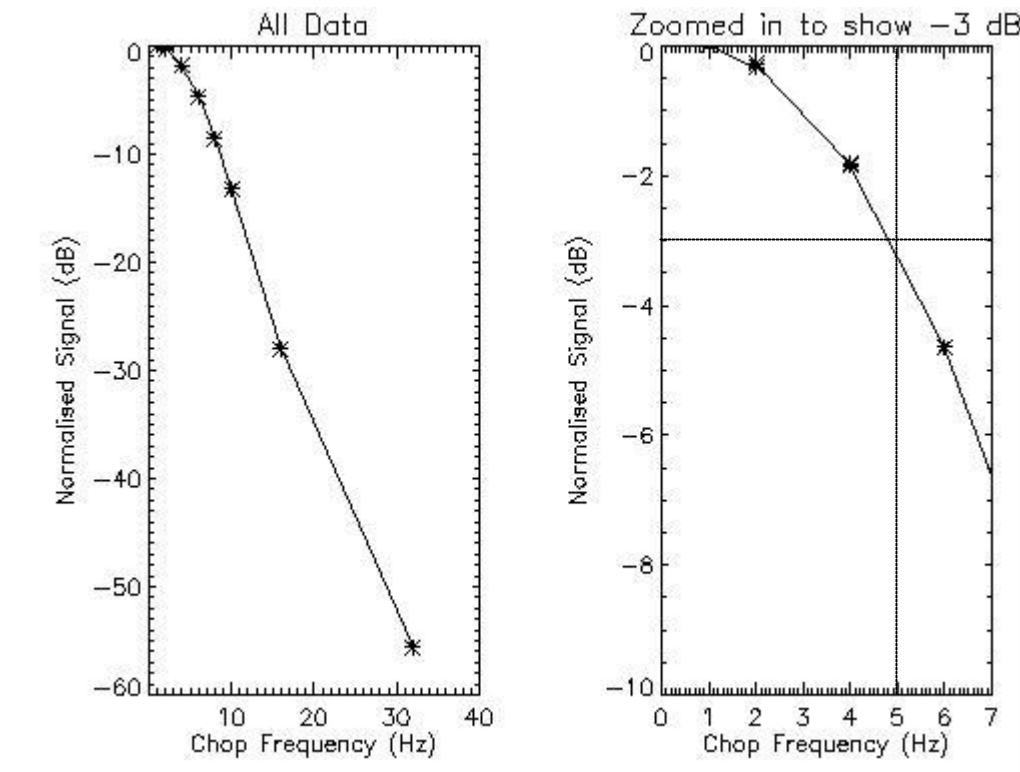
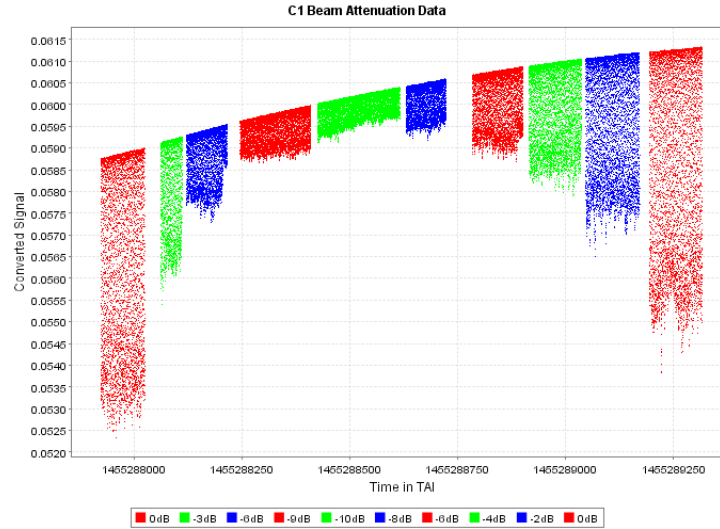


Figure 2.8: Response of pixel C5 to different modulation frequencies.

## 2.5 Linearity Test

The linearity, nominally of pixel C5, was measured by attenuating the signal from the laser beam in steps. The external chopper was used to provide signal modulation at 2 Hz and the filter (paper) attenuation was measured, using a Golay cell, to be 1 dB per sheet. Approximately one minute of data were taken at each attenuation level and the data were saved into separate files for each attenuation. The attenuation levels used were 0, -3, -6, -9, -10, -8, -6, -4, -2, and 0 dB.

Although the intention of this test was only to test a single pixel, the fact that the laser power reaching SPIRE was much higher than it should have been, meant that 26 pixels were illuminated sufficiently to obtain results although some pixels were saturated at the higher levels.



**Figure 2.10:** The raw linearity test data for pixel C1. Note that here signal is in the negative direction. This plot illustrates the drift in baseline due to temperature changes of the detectors following LHe refill of the cryostat. It also shows short period instabilities in the laser output which were still present following laser stabilisation.

This data reduction was performed using IA in JIDE. A new way of demodulating was coded to remove the uncertain baseline subtraction that is required for other methods. This method finds the peaks and the troughs in the data and calculates the difference between sequential peak-trough pairs. The mean value was then taken for each attenuation level of each detector. The data were plotted mean signal versus log dB level corresponding (in time order) to laser power changes of 1, 0.5, 0.25, 0.13, 0.1, 0.16, 0.25, 0.40, 0.63, 1.

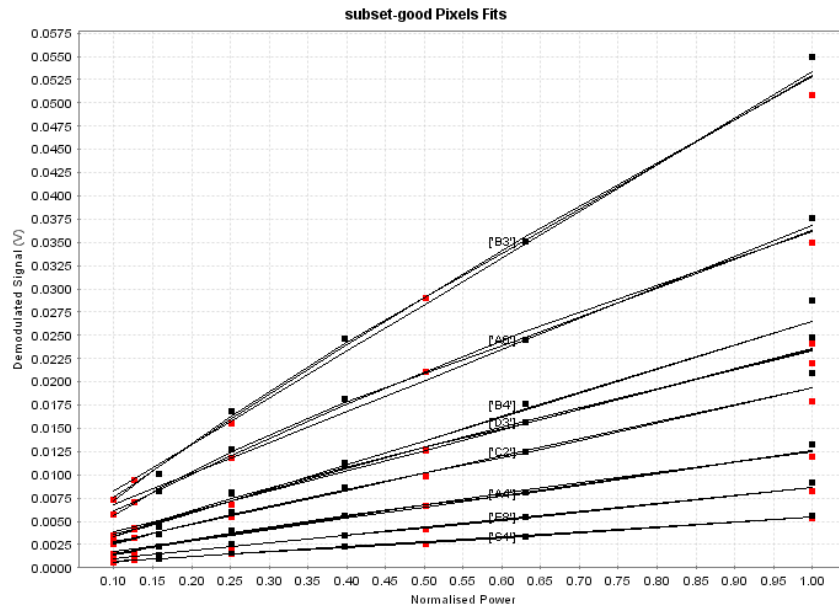


**Figure 2.11:** The demodulated signal from a selection of pixels versus the normalised power. The data from when the attenuation was being increased are shown in red. The black squares indicate the decreasing of the attenuation. The three lines show the results of fitting first, second and third order polynomials to the data.

The data look linear although there are departures and there may be hysteresis effects as well as that expectation that at high power levels the detectors will become non-linear.



For the next round of testing, more attenuation will be used and the baseline of single pixel illumination should be achieved. Further improvements can be gained by ensuring that the attenuation of all the filters used is measured, rather than extrapolating the measurements of some to all. Also an independent measure of the attenuated laser signal either via the Golay cell or by other means would be useful.

### 3 Optical Tests

Optical tests on the instrument were carried out with the internal flip mirror set to allow the instrument to view the ambient room background. Either the hot black body (HBB) or the laser can be used as an input source to telescope simulator. For HBB tests one of the light paths through the TFTS was blocked off and the signal was chopped at 2Hz by the external chopper. The HBB was set to 1200°C for all optical tests except where noted. For the initial set up of the telescope simulator the iris on the black body was opened to allow a broad area of the array to be illuminated. The telescope simulator was then scanned until the black body signal could be detected by the SPIRE array. Once the position was known, the offset from the expected position was then entered into the telescope simulator scan table, the iris was closed and the scan table was checked by placing the signal in turn on each of the pixels used for optical testing (see figure 1.1).

#### 3.1 Optical Cross Talk Test

In addition to providing a check on the scan table the set up data were also used for initial testing for optical crosstalk. The data were demodulated and corrected for optical efficiency variation across the array. Figure 3.1 shows the response of the array to illumination in E5. Although the analysis is not complete, as the variation in the detectors' responsivity has not yet been taken into account, it can be seen that any modulated signal from a non-illuminated pixel is within the noise level.

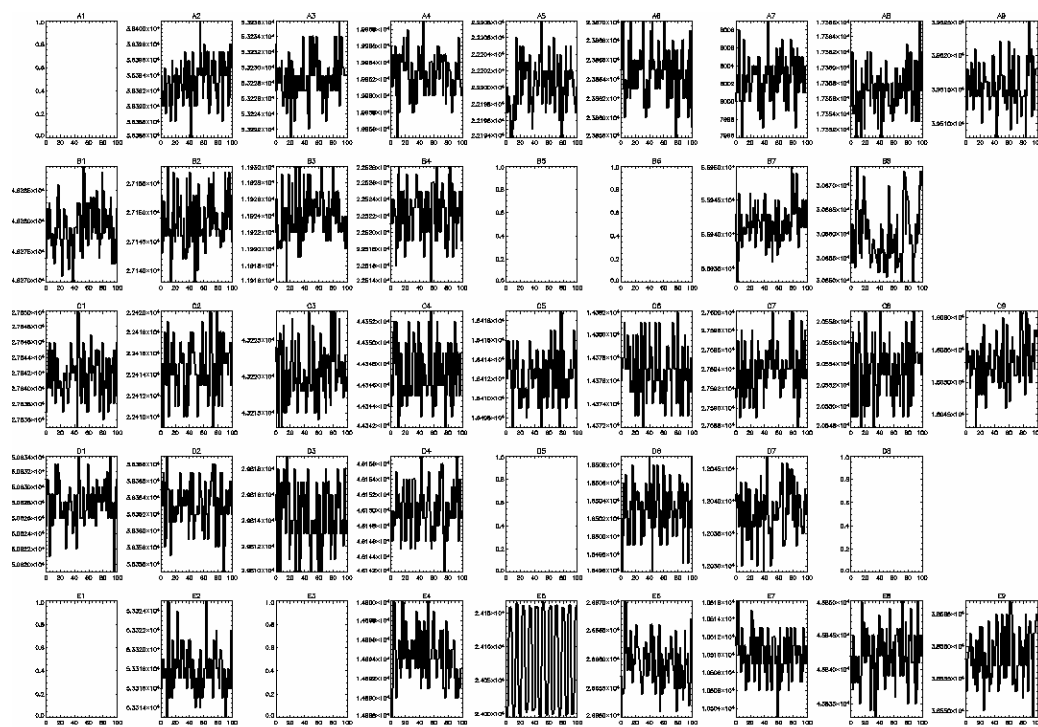


Figure 3.1: Signal on the array from optical crosstalk test for pixel E5. The first 100 points of data are shown and no signal is detected in pixels other than E5.





Following demodulation and optical efficiency correction, for all cases except C5, no modulated signal was detected in any non-illuminated detector. When C5 was illuminated a modulated signal at the level of about 4% of the signal in C5 was detected in D4. Further investigation using the PSF test data (see section 2.2) showed that this was due to the source not being centrally located in the pixel.

As performed this test only partially met the goal of performance testing for optical crosstalk. The instrument performance requirement is 1% for optical crosstalk and 0.5% for electrical, however the cut off for detecting modulated signal in any detector was at about 4% of the black body signal in the illuminated detector. This was due to the black body signal not being strong enough to provide sufficient contrast. In the next test campaign it should be possible to use the laser as the illuminating source, which will provide a much higher fidelity test.

### 3.2 Pixel Centre

The method of peak-up adopted involved placing the image of the HBB at the approximate position of the pixel with the telescope simulator, then doing a cross-scan of the pixel as shown in figure 3.2. At each position QLA was inspected and the signal was recorded by hand from the screen. Once the signal had been obtained the telescope simulator was moved to the next position. Peak-up was done on nine pixels as shown in Figure 1.1.

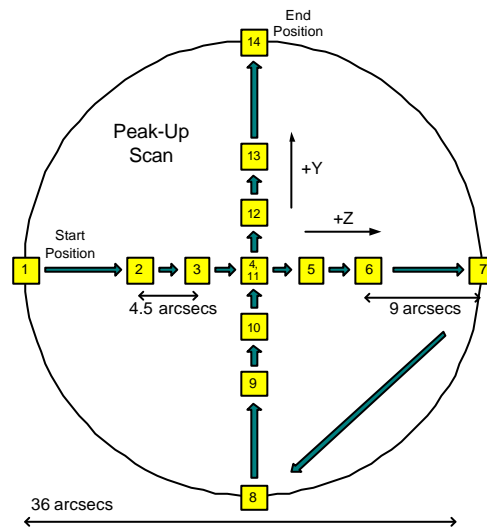


**Figure 3.2:** Cross-Raster adopted for peakup.

The peak-up data was then used to re-position the telescope simulator for further optical tests, in particular the spectral response tests.

Analysis of the PSF test (see next section) indicates that for pixel C5, this procedure was insufficient. For the next round of testing the following measures will be adopted.

1. Four extra points will be added i.e. between positions 1 and 2, 6 and 7 etc.
2. The peakup procedure will be done twice with the aim of confirming the applied offset.
3. If possible (i.e. time permitting) a QLA script will be developed to produce a more accurate measurement of the signal.





### 3.3 PSF Test

The PSF test was carried out by performing a raster scan of the HBB image across one pixel position. Only pixel C5 was tested; this took two hours taking two minutes of data taken at each of the 37 positions (see figure 3.3).

Prior to this scan, the peakup procedure had been done on C5 and the central location used for this test was that found by the peakup procedure. However the raw demodulated values shown in Figure 3.4, clearly show that the actual centre of the beam is a few arcseconds in the -Y direction from the centre found with the peak up procedure.

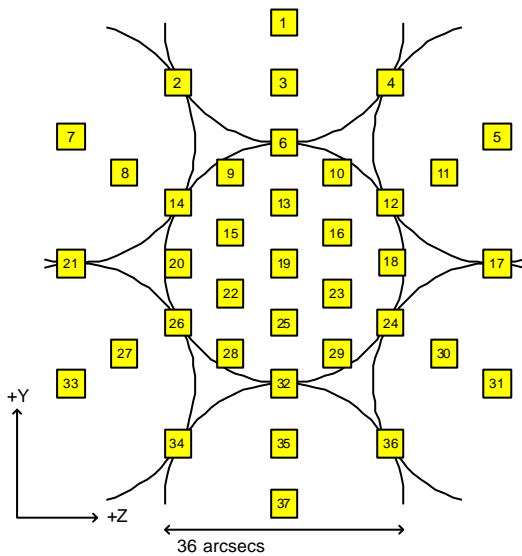


**Figure 3.3:** The raster positions used to do the PSF test.

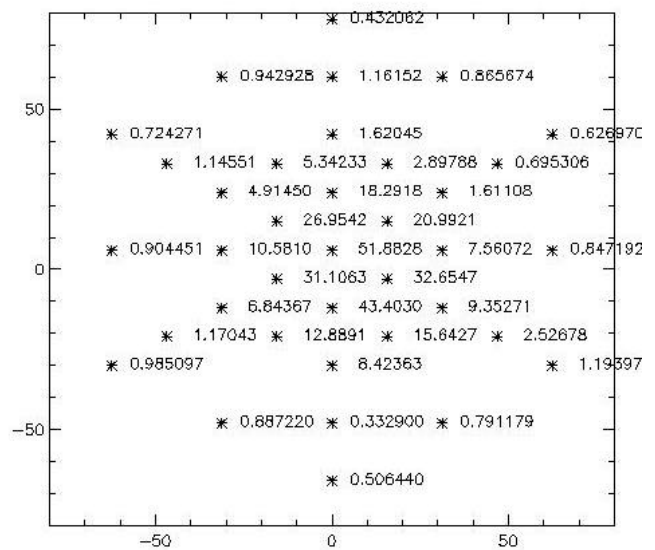



**Figure 3.4:** The raw demodulated values from the beam scan on C5.

The three directions where the beam was sampled 9 times were fitted using linear gaussian fits. The values obtained were FWHM = 39.2 arcseconds in the +Y-Z to -Y+Z direction, 37.4 (+Y to -Y), 35.5 (+Y+Z to -Y-Z). The average FWHM is therefore  $37.3 \pm 1.8''$ .

Based on the assumption that the PLW feedhorns are optimized for an  $\sim 8.7$  dB edge taper ( $1/e^2$  intensity on stop aperture edge), we expect the band-integrated (assuming theoretical rectangular profile for the in-band spectral response) Gaussian beam through the telescope simulator to be  $\sim 33.8$  arcsec FWHM. Possible explanations for the 10% increase difference seen in the data are a possible combination of the following effects:

- The feedhorn pattern is not tuned to  $\sim 8.7$  dB but higher edge taper i.e. there is a greater level of beam truncation at the limiting aperture such as the cold stop and telescope simulator pupil mask.
- Defocus - to explain the full difference one would need  $\sim 20$ mm defocus at the array plane, which is too high.
- Pupil and field misalignment at the interface between SPIRE (inside the cryostat) and the telescope simulator (outside the cryostat) and between the source and the telescope simulator.
- Residual aberrations from SPIRE optics, including filters and dichroics and cryostat window when under vacuum and at operating temperature.

	<h1>SPIRE Test Report</h1>	<b>Ref: SPIRE-RAL-REP-002083</b> <b>Issue: DRAFT</b> <b>Date: 14 July 2004</b> <b>Page: 17 of 17</b>
CQM Cold Test 1 Performance Test Report Editor: Bruce Swinyard		

Each of these factors could account for a few % difference. Therefore, assuming that the test beam was delivered within  $\pm 5$ mm to best BDA focus (i.e. not geometric focus but the long-wavelength band optimised focus), the measured FWHM from the beam pattern profile are well explained by the expectation from theory plus the few effects listed above. They may all realistically contribute to the broadening of PSF but at a level which remains small in total.

There will be several improvements to this test strategy for the post-vibration tests.

1. The improved peak-up procedure should provide better knowledge of the beam centre.
2. It is likely that instead of hexagonal sampling a square raster will be adopted. This will allow better 2-D fitting.
3. A fine cross-raster will be additionally tried so that 1-D Gaussians can be assessed against the 2-D case and to benchmark the use of this for other pixels in flight model testing.
4. More pixels will be tested as pickup data indicates possible vignetting effects at the edge of the array. The additional pixels will both be in the non-vignetted part of the array and the vignetted part.

It should be noted that this data could be used to look at the beams of other pixels. This analysis has not yet taken place.

### 3.4 Pupil Test

To carry out the pupil scan test, the optical bench was reconfigured so that the telescope simulator could scan the blackbody in the input pupil plane of the instrument. The scan was performed the same way than the scan of the focal plane, i.e. using the flat mirrors of the telescope simulator. The actuators used to control the movement of the flat mirrors did not have sufficient range to allow the full pupil to be scanned and about 75% of the pupil was scanned in Z. This set-up did not allow scanning in the instrument Y direction i.e. perpendicular to the bench plane.

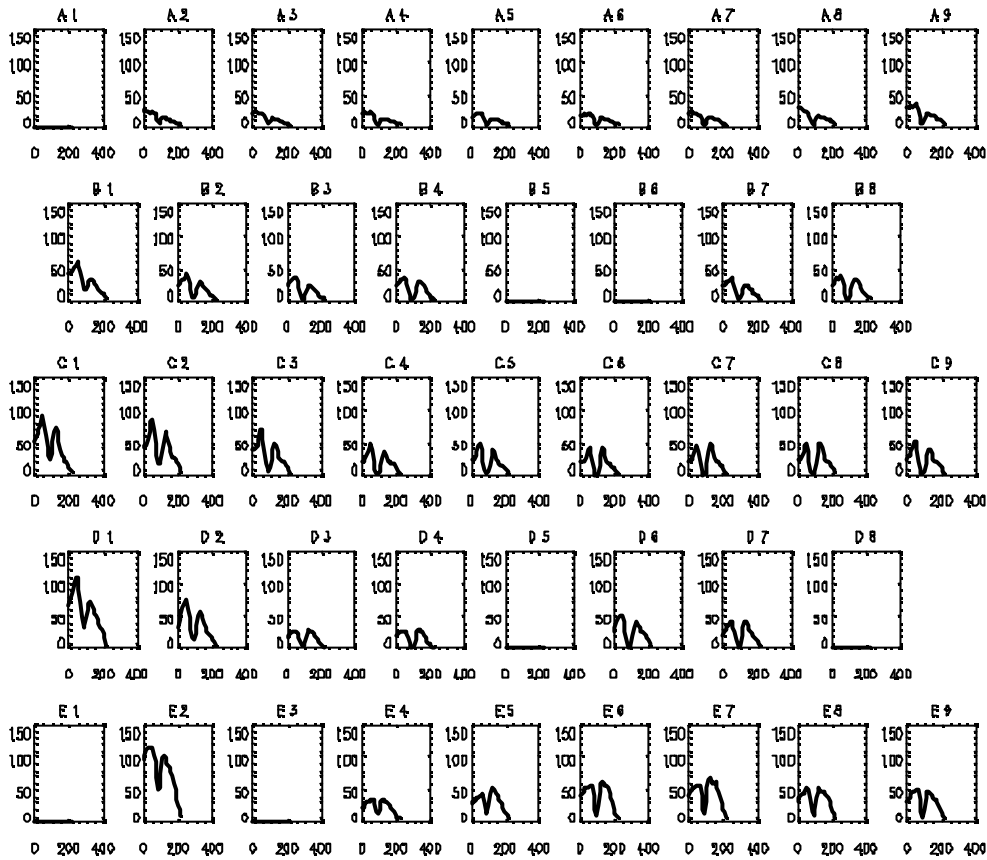
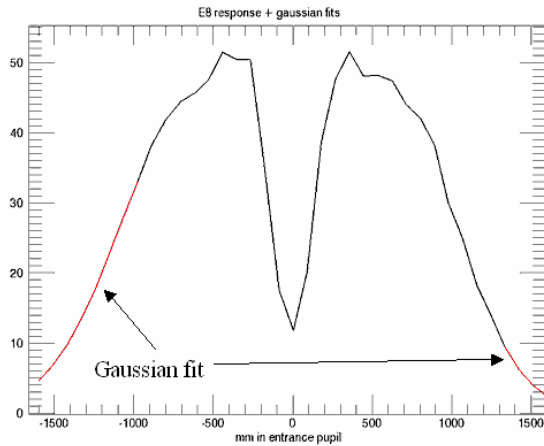


Figure 3.5: The array response to the black body as it is scanned across the pupil.

Figure 3.5 shows the scans in each of the detectors in the array. The figure clearly shows a ‘hole’ in the middle of the curve for each detector. This is due to the hole in the BSM mirror (for PCAL).

The overall array signal shows strong asymmetry with the average signal not constant across the array. This could be explained by vignetting and/or by a too small aperture of the beam but the exact cause of this is not fully understood and investigation of the optical setup following the test showed that the scan was performed starting from a misaligned position. This was due to a (non-planned) tilt of 0.5 deg on the mirror F3. This should result in a +29mm shift of the source in the pupil plane, however the centre was found to be at +40mm. The 11 mm shift that remains could be due to a misalignment of the telescope simulator with SPIRE but the asymmetry seems strong even on pixels on line C, which is not at an edge of the array, therefore there are probably further unidentified factors affecting this measurement.

To check the beam, pixel E8, which showed a symmetric response to the pupil scan was analysed further.



**Figure 3.6:** Pupil scan data for pixel E8. The missing parts are 'filled in' via a gaussian fit.

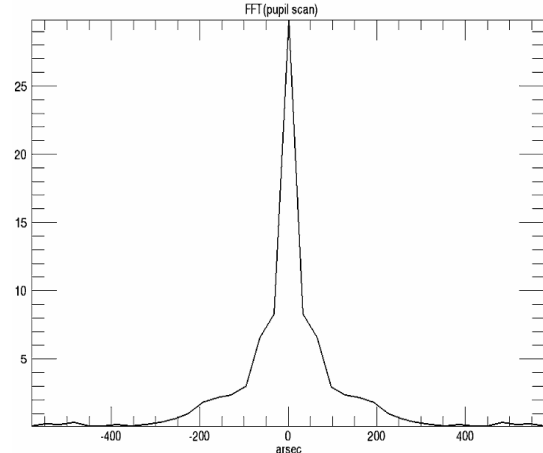


**Figure 3.7:** The beam for E8 obtained by transforming the pupil scan. The x-axis is arcsec on the sky.

The profile edges were used to fit a Gaussian (see figure 3.6) and this was then Fourier transformed to obtain the beam (see figure 3.7). The FWHM of the resultant beam was found to be about 50 arcseconds. This is far in excess of the almost nominal value found from the PSF test (see section 3.3) and can not be explained by widening due to the central obscuration alone and is probably due to a combination of effects described above.

Clearly this test was not sufficient to allow a good measure of the pupil. It is an important test because ideally it can give information about the beam in all pixels simultaneously and, provided that the source can be scanned away from the pupil, allow a determination of straylight. Therefore getting this test right for the next test campaign has been a priority. A new configuration where, instead of the blackbody being scanned by mirrors, it will be physically moved and the mirrors will remain fixed. This test will be done as early in the campaign as possible to allow sufficient time for assessment of the data and re-planning for a possible repeat towards the end of the test campaign.

### 3.5 Spectral Response

The spectral response of a single photometer pixel can be obtained by performing a number of scans of the hot blackbody with the test facility Fourier transform spectrometer (TFTS) See RD4 for details of the testing – here we summarise the results. The following tests were carried out:

1. 60 low resolution scans were performed with the telescope simulator set to the C5 peak-up position and the hot blackbody set to 1200°C. For this test the maximum OPD was 2 cm and the stage velocity was 1.0 mm/s – this was reduced for subsequent tests.
2. Sets of six high resolution scans were performed on pixel C5 at each of blackbody temperatures, 900°C and 1200°C. For this test the maximum OPD was 34 cm and the stage velocity was 0.5 mm/s.
3. Six low resolution scans were performed on each of pixels E5, A5, C1, C9, A9, E9, E2 and A2 with the hot blackbody set to 1200°C. For these tests the maximum OPD was 2 cm and the stage velocity was 0.5 mm/s.

The theoretical transmission spectrum of the TFTS was modelled to allow for comparison with experimental observations. The modelling should include a full radiative transfer analysis of all optical components from the blackbody, through the TFTS, and the optical path including the telescope simulator to the entrance window of the cryostat, but detailed understanding of each



component is not known so to a first approximation, it was assumed that the theoretical spectrum is given by the following relationship

$$S = F(SR)(\epsilon)(e^{-\tau})[B_h A \Omega - k]$$

where F is the filter profile, SR is the spectral response,  $\epsilon$  is the combined warm mirror efficiency,  $B_h$  is the Plank function for the 1200°C blackbody source,  $e^{-\tau}$  is the atmospheric transmission, and A is the detector area, and  $\Omega$  is the detector solid angle.  $\Omega$  is expected to be proportional to  $\lambda^2$  due to the single mode propagation. In addition there is another factor, k, to include to account for radiation between the cryostat window and TFTS. This factor can be accounted for by using two blackbody temperatures but assumptions of flatness was assumed when only one temperature was available.

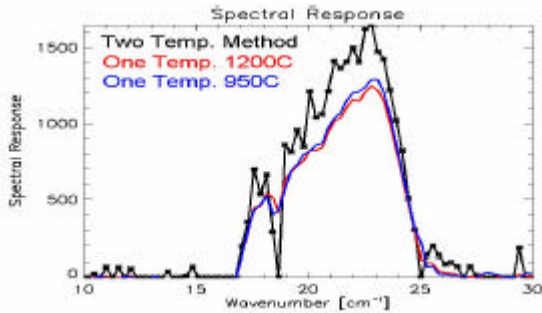


Figure 3.8: Spectral response determined for pixel C5 using both black body temperatures then individually assuming an approximation for k.

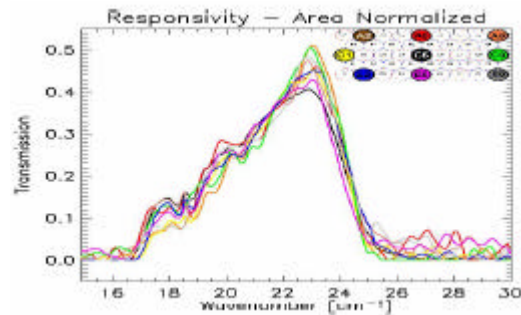


Figure 3.9: Spectral responses of the nine pixels tested with a flatness approximation for k.

Figure 3.8 shows the result of this approximation for C5, the only pixel where two temperatures are available. The spectral bandpass of C5 is then compared with the other pixels tested in figure 3.9. Although noisy the bandpass obtained from the high resolution data matches that obtained with the low resolution data. The band passes of all pixels are, as expected in good agreement with each other. However the measured bandpass is not in accord with that predicted from the product of the filters – see figure 3.10 – this is still under investigation.

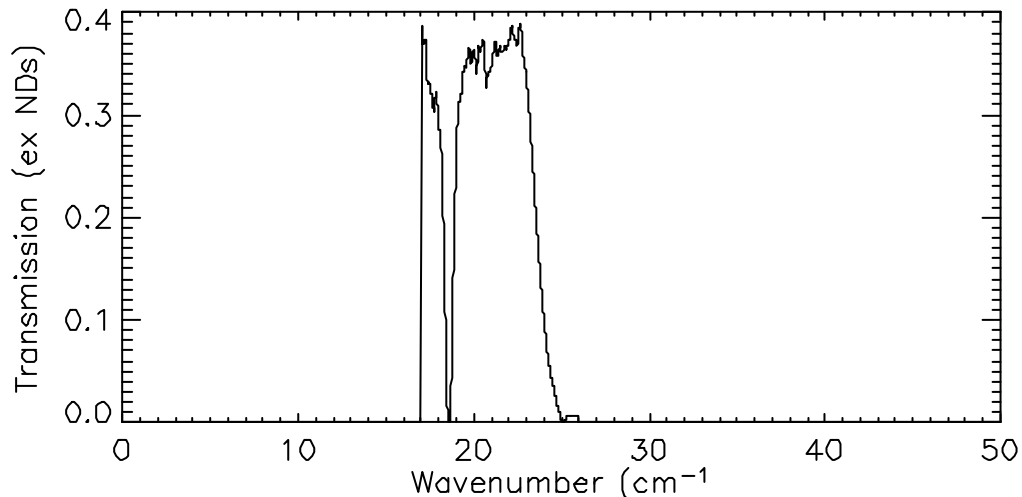
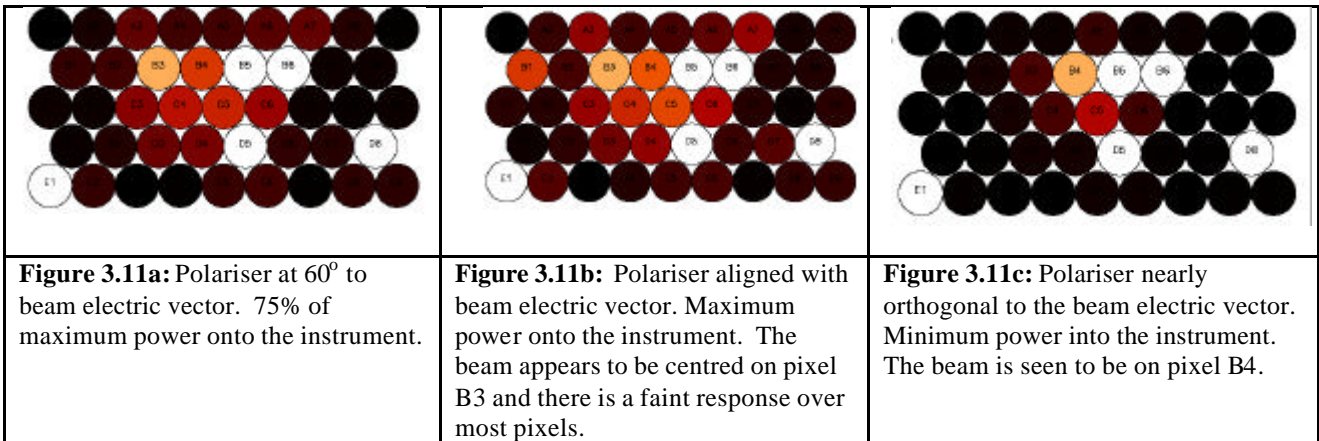


Figure 3.10: The predicted spectral response from the combination of the SPIRE filters. The measured bandpass has a pronounced roll off towards lower frequencies which is not as yet understood.

	<h1 style="margin: 0;">SPIRE Test Report</h1>	<b>Ref: SPIRE-RAL-REP-002083</b> <b>Issue: DRAFT</b> <b>Date: 14 July 2004</b> <b>Page: 21 of 21</b>
CQM Cold Test 1 Performance Test Report Editor: Bruce Swinyard		

### 3.6 Polarisation

Use of the laser for testing was restricted during the initial test campaign due to time constraints. The major issue discovered was that the power from the laser quickly saturated the bolometers. This is illustrated in figure 3.11, which shows the bolometer array response as a polarising grid is rotated in the beam – the laser output is inherently polarised therefore this reduces the power. We can see that the apparent position of the beam moves as the individual detectors start to respond correctly rather than saturating. We can also see that, when a very large amount of power is incident on the instrument there are indications that one edge of the array (the upper one in figure 3.11) is illuminated preferentially. This seems to be due to a glint from the SPIRE structure close to the entrance focal plane, the CQM was built without the full straylight control measures and we expect this issue to be solved for the flight model by the use of absorbing material around the focal plane baffle.



### 3.7 Focus Test

Once the hot blackbody source position with respect to the array had been determined (see above), this was used to illuminate the central pixel. The focus of the telescope simulator was then adjusted manually while the modulated signal was monitored via the QLA system. This test proved difficult to perform as hystereses in the telescope simulator system meant that it was not easy to position the mirrors precisely and repeatably. However the signal is fairly insensitive to exact focussing due to the slow beam and the position found proved satisfactory for all subsequent testing.

## 4 PCAL Tests

### 4.1 PCAL Level Response

The PCAL level response test was designed to both characterise the response of the detectors to different commanded PCAL levels and to determine the minimum level of PCAL that would be detected. The level test was run three times during the test campaign with each test run taking about 15 minutes.



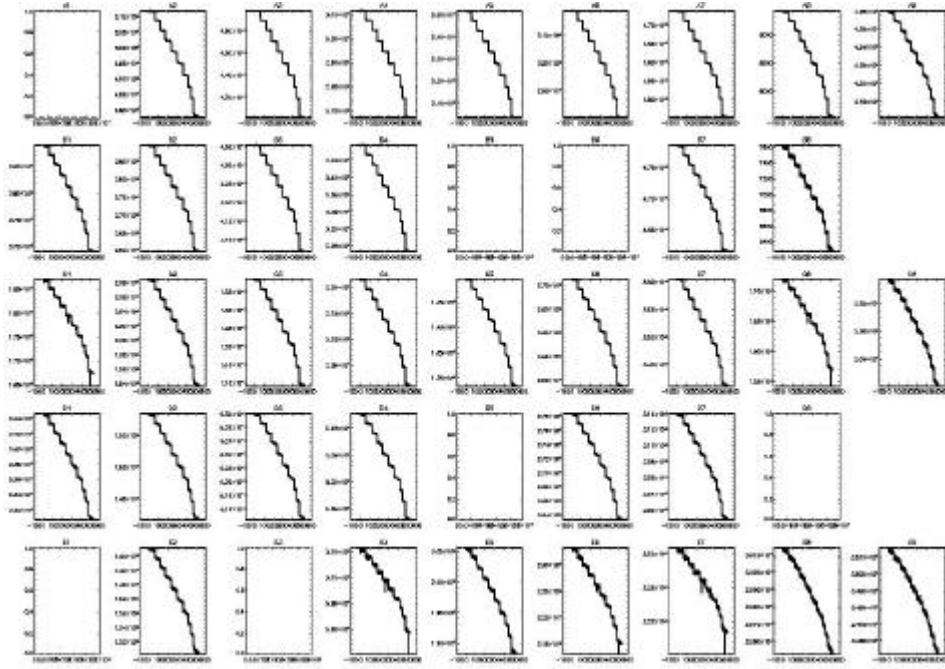


Figure 4.1: The response of the array to the PCAL level test.

The PCAL was set to each of 18 equidistant levels between zero and its maximum range in turn and the response of the array to this is shown in figure 4.1. As the location of PCAL is within the BSM the illumination is from the pupil. Hence the illumination from PCAL is distributed across the array and the signal is not chopped except by directly commanding PCAL.

The reason that this test was done three times was that during the first two occasions large drifts in detector temperatures were noted and it was thought that this was due to the drifts associated with the LHe running out. However the conditions were stable during the third run of this test and large changes of temperature were still noted. This is probably due to the thermal dissipation from the highest level settings of PCAL disturbing the system. As this was not found when a simulated chop signal was applied (see section 4.2), this test will not be repeated in its current form and a return to zero level will be applied between each PCAL level. However as signal was observed even at the lowest level the only need for repeating this test is for post-vibration verification and this could be done from the frequency test alone.

## 4.2 PCAL Frequency Response

The aim of the PCAL frequency response test was to attempt to set up PCAL for use as the internal calibration source. To do this PCAL was commanded between two levels and the frequency associated with the level change was embedded in the commanding via a virtual machine in the on-board software (OBS). Two attempts at doing this test had to be aborted before the test was run successfully on 12/02/2004. The test sequence consisted of testing a pair of levels at 5 different frequencies, 4, 2, 1, 0.5 and 0.25 Hz. Only two level pairs were tested, 0 to full level (7 mA) and 0 to half level (3.5 mA).



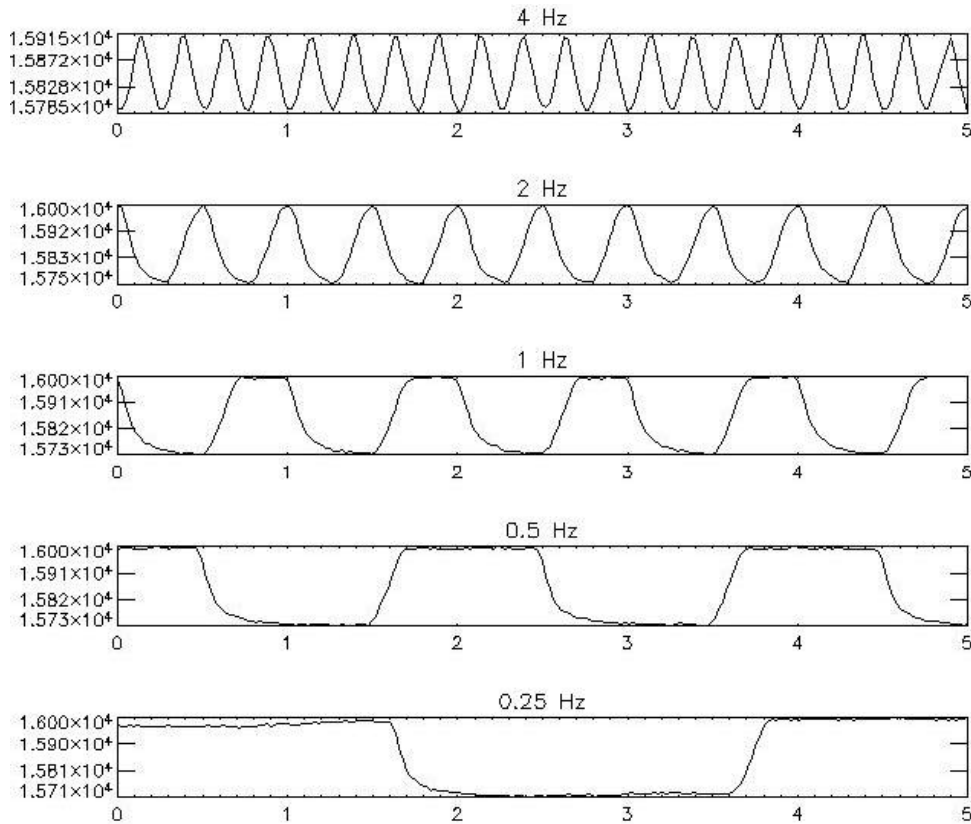
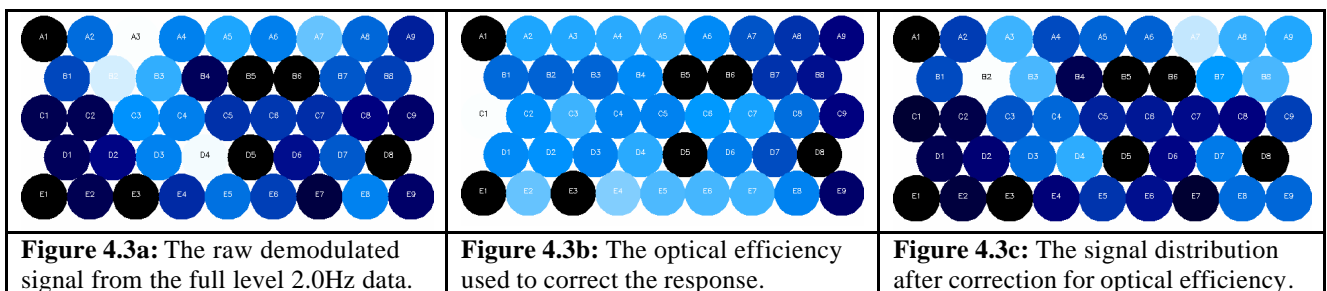


**Figure 4.2:** The response of one detector to the five frequencies tested at the max level change.

Figure 4.2 shows the response of one detector to the five frequencies tested for the 0-7 mA test. It is clear that for all frequencies except the 0.25 Hz frequency, time constant effects mean that the level is not being reached. This is not due to time constants in the detectors themselves but rather time constants in the CQM PCAL which did not meet flight specification. The same result was obtained for both level pairs tested.



One of the purposes of this test is to investigate how PCAL illuminates the array. To do this the signal was demodulated then the optical efficiency was accounted for. Figure 4.3a shows the array raw response, figure 4.3b shows the optical efficiency distribution that was used for correction (see section 2.4, the JPL derived optical efficiencies were used), and figure 4.3c shows the illumination pattern after optical efficiency correction. All frequencies tested show this illumination pattern. This is not the final result as the differences in detector responsivity have not yet been accounted for. However there is a hint of the same illumination pattern as observed in the polarisation test i.e. a glint may be affecting the top row in both figures 3.11 and 4.3.



It would have been desirable to explore a larger parameter space but unfortunately the lateness of getting the test working meant that this could not be done. There are several changes that will be implemented for the next round of testing...

1. Characterisation – a larger parameter space will be explored.
2. Do more often – a subset of this test will be done on a regular basis, this is to start using PCAL as a calibration source.
3. Associate the PCAL data more closely with the detector data. This will be done via regular PCAL flashes associated with load curves.
4. Understand the PCAL output – we will take load curves at set PCAL outputs.

## 5 Harness Tests


### 5.1 Microphonics Test

The detector was biased at peak sensitivity (~13.5 mV for P/LW) with DC bias through the redundant wire connections. The signals from the DC amplifier chain were recorded through the spectrum analyzer. With the spectrum analyzer set to average about 10 traces in peak mode to record signal increases the data were recorded. Note there are a forest of lines due to mains and harmonics, plus a series of unidentified frequencies (UIFs), seen up to 225 Hz. The dewar was tapped on one of the HOB support feet with a screwdriver handle and another spectrum recorded.

Microphonics appear at 230 – 325 Hz, 450 – 500 Hz, and 820 – 950 Hz. Only a few channels were tested. The sensitivity to microphonics was significantly different for each channels for unknown reasons. Testing more channels in the future would be a good idea. Note the “BoDAC noisy” pixel showed a significant response at low frequencies. This is probably due to a contact noise mechanism in these pixels, as they characteristically displayed contact 1/f noise when readout through the DRCU.

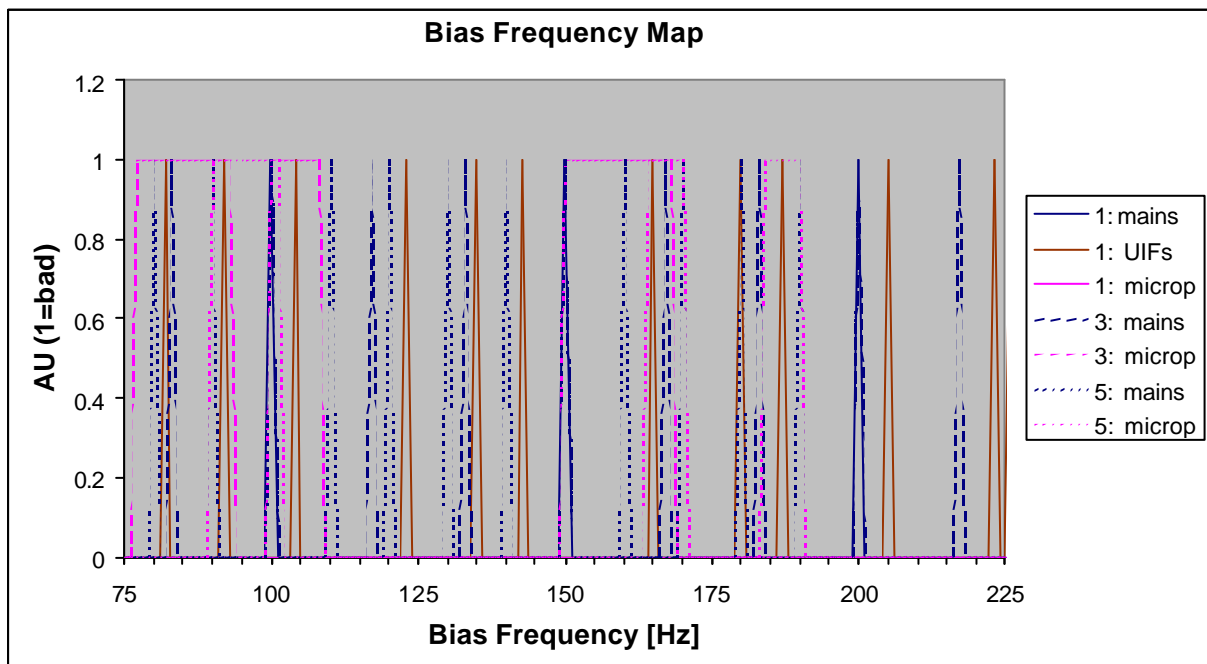


**Figure 5.1:** Made frequency map for the CQM PLW made by tapping the test cryostat

	<h1>SPIRE Test Report</h1>	<b>Ref: SPIRE-RAL-REP-002083</b> <b>Issue: DRAFT</b> <b>Date: 14 July 2004</b> <b>Page: 25 of 25</b>
CQM Cold Test 1 Performance Test Report Editor: Bruce Swinyard		

A bad frequency map was made by considering the response to mains, UIFs, and microphonics at the bias frequency and aliased odd harmonics. The plot (figure 5.1) shows this response up to 5<sup>th</sup> harmonic, however the highest harmonic frequency depends on the filtering prior to lockin. The measured cable rolloff is ~600 Hz (3 dB) for dark bolometers at low bias. In flight, this rolloff frequency may go up to ~1000 Hz. The analog bandpass filter in the DRCU also limits the high frequency response.

Aside from the issue of mains pickup and RC rolloff, the best frequencies for avoiding microphonics appear to be 120 – 140 Hz, 175 Hz, and 200 – 220 Hz. This test is far from conclusive but has proven that the technique is feasible for detecting microphonic susceptibility in SPIRE. We will repeat the test in a more quantitative way on the next cooldown.

## 5.2 Harness Test

The procedure for testing the harness used a non-standard set up with the bias supplied by GSE and a Hewlett-Packard spectrum analyser connected to the output via a GSE DC amplifier card.

The outline procedure was as follows:

- Turn off power to DRCU
- Disconnect J14, J15, and J16 from DRCU electronics.
- Connect selected cable (J14, J15, or J16) to breakout box.
- Supply DC preamp with +/- 9V; it has a gain of 375, flat to > 1 kHz.
- Run selected channels from breakout to input of DC preamp as desired using (disconnected) redundant bias cable.
- Leave prime bias cable connected to DRCU.
- Turn on power to DRCU and turn on JFETs.
- Set DRCU bolometer bias to zero.

### 5.2.1 JFET Vs checkout.


This was a measurement of the source voltages on all JFETs. This procedure confirms that the JFETs are working properly, as the values should match measurements at JPL. The differential outputs should be closely matched in voltage. The results show that all 48 JFETs are operating properly.

### 5.2.2 Cable RC rolloff test.

The first task in checking the JFET to BDA harness was to confirm that using DC supply can supply bias by applying 25 mV and looking at output of an open channel. It should show ~24 mV differential change. The output impedance of the DRCU bias supply is 4000 ohms, so a bias generator with low output impedance will control bias at the detector to within a small correction factor. Apply 5 mV pulsed chirp through redundant supply lines, and measure transfer function with the DC preamp and spectrum analyzer. The spectrum analyzer also can plot relative phase shift.

Result: The open channel shows a 3dB reduction at 173 Hz. Bolometers (dark, 3He fridge at 265 mK) show a rolloff point at 580 – 700 Hz. The total phase shift is less than 15 degrees at 160-200 Hz for the bolometers.

The circuit may be modeled as an effective impedance  $R_{\text{eff}}^{-1} = R_{\text{bol}}^{-1} + (20M)^{-1}$ , where the total load resistor impedance is about 20 MOhms, with an effective parallel capacitance C. The open channel test shows a reasonable value for C = 45 pF. The bolometer channels give somewhat higher rolloff frequencies than expected, assuming a calculated value for dark detectors at 5 mV bias. Perhaps the

	<h1>SPIRE Test Report</h1>	<b>Ref: SPIRE-RAL-REP-002083</b> <b>Issue: DRAFT</b> <b>Date: 14 July 2004</b> <b>Page: 26 of 26</b>
CQM Cold Test 1 Performance Test Report Editor: Bruce Swinyard		

detector impedance is lower than calculated due to optical loading or incorrect estimate of the BDA temperature.

Generally it is good practice to keep the phase shift small. A maximum of 15 degrees of phase shift is a reasonable rule of thumb, in order to reduce susceptibility to capacitance fluctuations (a type of microphonic susceptibility). At 15 degrees phase shift, the attenuation of the signal amplitude is small, about 3.5 %. For the dark bolometer case, to keep the phase shift less than 15 degrees at peak sensitivity, the bias frequency should be < 120 Hz. Under conditions of increased bias and/or optical loading, the detector impedance will be lower and the cable RC rolloff will be less of an issue. For the optically loaded case, with a base temperature of 310 mK, the phase shift will be less than 15 degrees at peak sensitivity if the bias frequency is < 220 Hz. Depending on the flight loading conditions, operating temperature, and microphonic environment, more or less bias frequency space will be available.

## 6 Tests Not Done

### 6.1 Straylight Test

It was originally intended to measure the out of field straylight by putting a source just outside the FOV of SPIRE. The test equipment setup did not allow this test to be made and it is unlikely that this situation will change. Instead a measure of the straylight was obtained in the following ways...

1. Load Curves (see sections 1.3) – The dark load curves gave results for the bolometer parameters which were very similar to those obtained from detector testing indicating no straylight in the dark environment.
2. Optical Efficiency (see section 1.4) - The pattern of optical efficiency obtained from the optical load curves is well matched to that obtained during detector testing, again indicating no significant areas of the array affected by straylight.
3. Optical Crosstalk Test (see section 1.5) – Although inconclusive, this test showed no crosstalk above the 4% level. Once the laser power is reduced a higher fidelity test will be done in the next round of testing.
4. Pupil Scan (see section 2.3) – This test is in-principle capable of making a direct measurement of out of field straylight but unfortunately the CQM pre-vibration test setup did not allow this. The updated test will allow this to be measured for the Z axis.
5. Polarisation Test (see section 2.5) – Although this test was not intended to measure straylight, the fact that the laser power was so high did allow the detection of a possible glint on one side of the array. This glint is probably due to an undersized aperture in the test equipment rather than any effect due to the instrument itself.

### 6.2 Out of Band Radiation Test

The dedicated out of band radiation test was the only test not done due to time constraints. This test consists of comparing radiation from an in-band laser line with that obtained from out of band laser lines and it will be done in the next test campaign, as a low priority test, provided time is available. Although the dedicated test was not done, confidence has been gained that the SPIRE out of band rejection is good from the results of the spectral response test. The use of an FTS to make this measurement allowed the spectral response to be determined down to  $50 \text{ cm}^{-1}$  ( $200 \text{ }\mu\text{m}$ ) and no out of band radiation was detected.



## SPIRE Test Report

**Ref:** SPIRE-RAL-REP-002083

**Issue:** DRAFT

**Date:** 14 July 2004

**Page:** 27 of 27

CQM Cold Test 1 Performance Test Report

Editor: Bruce Swinyard

### 6.3 EMC Tests

Attempts to measure the effect of modulating the current through the dummy BSM coils were inconclusive as it proved difficult to use the QM0 MCU to do this test. We will attempt to repeat it using a signal generator during the next cooldown. We will also attempt the "field to wire" simulation by injecting signal directly onto the internal harness shield.